Molecular Systems Biology 9; Article number 704; doi:10.1038/msb.2013.56
Citation: ***Molecular Systems Biology*** **9:704**
www.molecularsystemsbiology.com

molecular systems biology

Promoter decoding of transcription factor dynamics involves a trade-off between noise and control of gene expression

Anders S Hansen[1,2,3] and Erin K O'Shea[1,2,3,4,*]

[1] Department of Chemistry and Chemical Biology, Harvard University, Cambridge, MA, USA, [2] Howard Hughes Medical Institute, Harvard University, Cambridge, MA, USA, [3] Faculty of Arts and Sciences Center for Systems Biology, Northwest Laboratory, Harvard University, Cambridge, MA, USA and [4] Department of Molecular and Cellular Biology, Harvard University, Northwest Laboratory, Cambridge, MA, USA
* Corresponding author. Northwest Laboratory, Faculty of Arts and Sciences, Center for Systems Biology, Harvard University, 52 Oxford Street, Cambridge, MA 02138, USA. Tel.: +1 617 495 4328; Fax: +1 617 496 5425; E-mail: erin_oshea@harvard.edu

Received 7.8.13; accepted 24.9.13

Numerous transcription factors (TFs) encode information about upstream signals in the dynamics of their activation, but how downstream genes decode these dynamics remains poorly understood. Using microfluidics to control the nucleocytoplasmic translocation dynamics of the budding yeast TF Msn2, we elucidate the principles that govern how different promoters convert dynamical Msn2 input into gene expression output in single cells. Combining modeling and experiments, we classify promoters according to their signal-processing behavior and reveal that multiple, distinct gene expression programs can be encoded in the dynamics of Msn2. We show that both oscillatory TF dynamics and slow promoter kinetics lead to higher noise in gene expression. Furthermore, we show that the promoter activation timescale is related to nucleosome remodeling. Our findings imply a fundamental trade-off: although the cell can exploit different promoter classes to differentially control gene expression using TF dynamics, gene expression noise fundamentally limits how much information can be encoded in the dynamics of a single TF and reliably decoded by promoters.

Molecular Systems Biology **9**: 704; published online 5 November 2013; doi:10.1038/msb.2013.56
Subject Categories: chromatin & transcription; signal transduction
Keywords: gene regulation; gene expression noise; microfluidics; Msn2; transcription factor dynamics

Introduction

To survive in a changing environment, cells must be able to sense the environment and transmit this information through signal transduction cascades to transcription factors (TFs), which then initiate a suitable gene expression response. Whereas downstream responses to signaling have typically been understood as consequences of the strength or amplitude of the signal, emerging evidence suggests that additional information can be encoded in the temporal dynamics of these signals (Behar and Hoffmann, 2010; Purvis and Lahav, 2013).

Several mammalian TFs exhibit complex and signal-dependent dynamics. For example, NF-κB, involved in controlling inflammation, undergoes nucleocytoplasmic oscillations in response to tumor necrosis factor-α (TNFα), but sustained nuclear localization in response to bacterial lipopolysaccharides (LPSs) (Nelson *et al*, 2004; Covert *et al*, 2005; Werner *et al*, 2005). Thus, NF-κB translocation dynamics encode the signal identity (TNFα or LPS). Similarly, the tumor suppressor TF p53 undergoes a dose-dependent number of nuclear pulses in response to DNA breaks, but a single sustained pulse with dose-dependent amplitude and duration in response to UV irradiation (Lahav *et al*, 2004; Batchelor *et al*, 2011). Thus, p53 dynamics encode both the dose (severity) and the identity of the stress. Similarly, two TF isoforms of NFAT also exhibit distinct dynamics in response to different stimuli (Yissachar *et al*, 2013).

The activities of budding yeast TFs also appear to be dynamically regulated. In response to calcium, the TF Crz1 exhibits short bursts of nuclear localization, where the duration is fixed but the frequency is dose-dependent (Cai *et al*, 2008). Msn2, a zinc-finger TF and regulator of the yeast multi-stress response, also exhibits oscillatory translocation dynamics (Jacquet *et al*, 2003; Petrenko *et al*, 2013). The identity and dose (severity) of three distinct stresses are encoded in the translocation dynamics of Msn2: in response to glucose starvation, Msn2 exhibits short bursts of nuclear localization with dose-dependent frequency; in response to osmotic stress, Msn2 translocates to the nucleus with a single initial peak with dose-dependent duration; and in response to oxidative stress, Msn2 shows sustained nuclear localization with dose-dependent amplitude (Hao and O'Shea, 2012).

Although it is clear that diverse signals are encoded in the dynamics of NF-κB, p53, NFAT, Crz1, Msn2, and many other TFs (Purvis and Lahav, 2013), we understand little about how

these signals are decoded by gene promoters and converted into gene expression programs. For example, do genes differ in their sensitivity to TF dynamics? And if so, what are the quantitative principles that govern this input–output relationship? Studies suggest that TF dynamics can influence the gene expression response. For example, p53 dynamics may affect cell fate through differential gene regulation: p53 pulses induce only DNA repair genes, whereas a single, sustained p53 pulse leads to higher expression of senescence genes (Purvis *et al*, 2012). Similarly, whereas some NF-κB target genes filter out low TNFα concentrations, others activate fully even in response to low TNFα concentrations (Ashall *et al*, 2009; Giorgetti *et al*, 2010; Tay *et al*, 2010). In the case of Crz1, as the frequency of nuclear localization bursts increases, the ratio of the majority of the induced genes is held constant as the gene expression increases (Cai *et al*, 2008).

In most previous studies, distinct stimuli (e.g., TNFα or LPS) were required to induce distinct TF dynamics (e.g., oscillations or a sustained pulse); since these stimuli can activate a large number of other factors or responses, it is difficult to establish that differential gene regulation is caused by TF dynamics instead of just being correlated with TF dynamics. To overcome this limitation, we previously developed a chemical genetic system that permits direct control of Msn2 translocation dynamics. Using this experimental set-up and modeling studies, we investigated how Msn2 dynamics affects expression of a single synthetic reporter gene and predicted that promoter activation kinetics influence the response to dynamic TF inputs (Hao and O'Shea, 2012). However, the extent to which different promoters can differentially decode Msn2 dynamics is not clear.

Moreover, previous studies used population-averaged techniques (e.g., qPCR or microarrays) that cannot provide information about the effect of TF dynamics on gene regulation in individual cells. This is an important limitation because gene expression is a stochastic process, such that surprisingly large differences can exist between otherwise genetically identical cells (Elowitz *et al*, 2002; Raser and O'Shea, 2004; Newman *et al*, 2006; Raj *et al*, 2006; Raj and van Oudenaarden, 2008; Lionnet and Singer, 2012). Although cells can exploit noise in gene expression through bet-hedging such as in bacterial persistence (Balaban *et al*, 2004), noise is by and large detrimental to the cell: given a particular signal, a specific gene expression response is generally optimal. Thus, even if information about signal dose and identity can reliably be encoded in TF dynamics, the information transfer will be fundamentally limited by the fidelity with which TF dynamics is subsequently decoded by promoters (Brennan *et al*, 2012). Hence, to understand how much of the information encoded in TF dynamics is lost due to gene expression noise, a detailed single-cell study is required.

To explore and understand the relationship between TF dynamics, gene expression and noise in gene expression output, we develop a method integrating high-throughput microfluidics and quantitative time-lapse microscopy to artificially control the translocation dynamics of Msn2 and measure gene expression of several Msn2 target genes at the single-cell level. Combining modeling and experiments, we predict and verify that by controlling Msn2 dynamics it is possible to differentially express genes. We show that, in theory, four different promoter classes are possible such that four gene expression programs can be encoded in the dynamics of a single TF. We find that, in general, oscillatory TF input leads to higher noise than single pulse input and also that some promoter classes exhibit dramatically higher levels of noise in gene expression than others as a result of a slow promoter transition step, which we show is related to slow promoter nucleosome remodeling. Thus, there is a trade-off between achieving low noise and differential gene expression. Taken together, we provide a systematic dissection of the extent to which TF dynamics controls gene expression and noise.

Results

Identification of specific target genes of Msn2

We employed a chemical genetic strategy to control the nuclear localization and activity of Msn2 (Bishop *et al*, 2000; Hao and O'Shea, 2012). Msn2 localization is regulated by protein kinase A (PKA)—when PKA is active, Msn2 is phosphorylated and cytoplasmic; when PKA is inhibited, Msn2 is unphosphorylated and localized to the nucleus (Gorner *et al*, 1998). We introduced analog-sensitive mutations (PKA^{as}) into all three catalytic isoforms of PKA (Tpk1, Tpk2, and Tpk3), which enabled us to selectively and reversibly inhibit PKA activity, and therefore control Msn2 localization, with the small molecule 1-NM-PP1 (Zaman *et al*, 2009; Hao and O'Shea, 2012). To quantify Msn2 localization, we introduced into the PKA^{as} strain an Msn2-mCherry fusion protein and a nuclear marker (Nhp6a-iRFP; Supplementary Figure S1A). To identify Msn2-specific target genes, we used microarrays to compare the gene expression response to 1-NM-PP1 in strains with and without Msn2-mCherry and identified 23 genes that showed at least five-fold upregulation in the presence of Msn2-mCherry, but no expression change in an *msn2*Δ strain (Supplementary Figure S1C). To measure both gene expression and intrinsic and extrinsic noise components, we chose seven of the most strongly induced of these genes and implemented the dual-reporter strategy (Elowitz *et al*, 2002), replacing the native ORF with fast-maturing CFP and YFP reporters on homologous chromosomes in diploid yeast cells. Finally, although PKA^{as} inhibition might have indirect global effects on gene expression, Msn2 directly controls the transcriptional response of these seven genes: they are not induced in the absence of Msn2 and previous genome-wide ChIP experiments have shown that Msn2 directly binds their promoters (Huebert *et al*, 2012).

Systematic dissection of how different promoters decode TF dynamics

To systematically investigate how induction of these seven Msn2 target genes depends on Msn2 nuclear translocation dynamics, we developed a high-throughput microfluidic device (Figure 1A). We used this device to rapidly switch between medium with and without 1-NM-PP1 and artificially modulate Msn2 nuclear localization, enabling us to control and measure Msn2 input dynamics and simultaneously measure gene expression output dynamics for >100 000

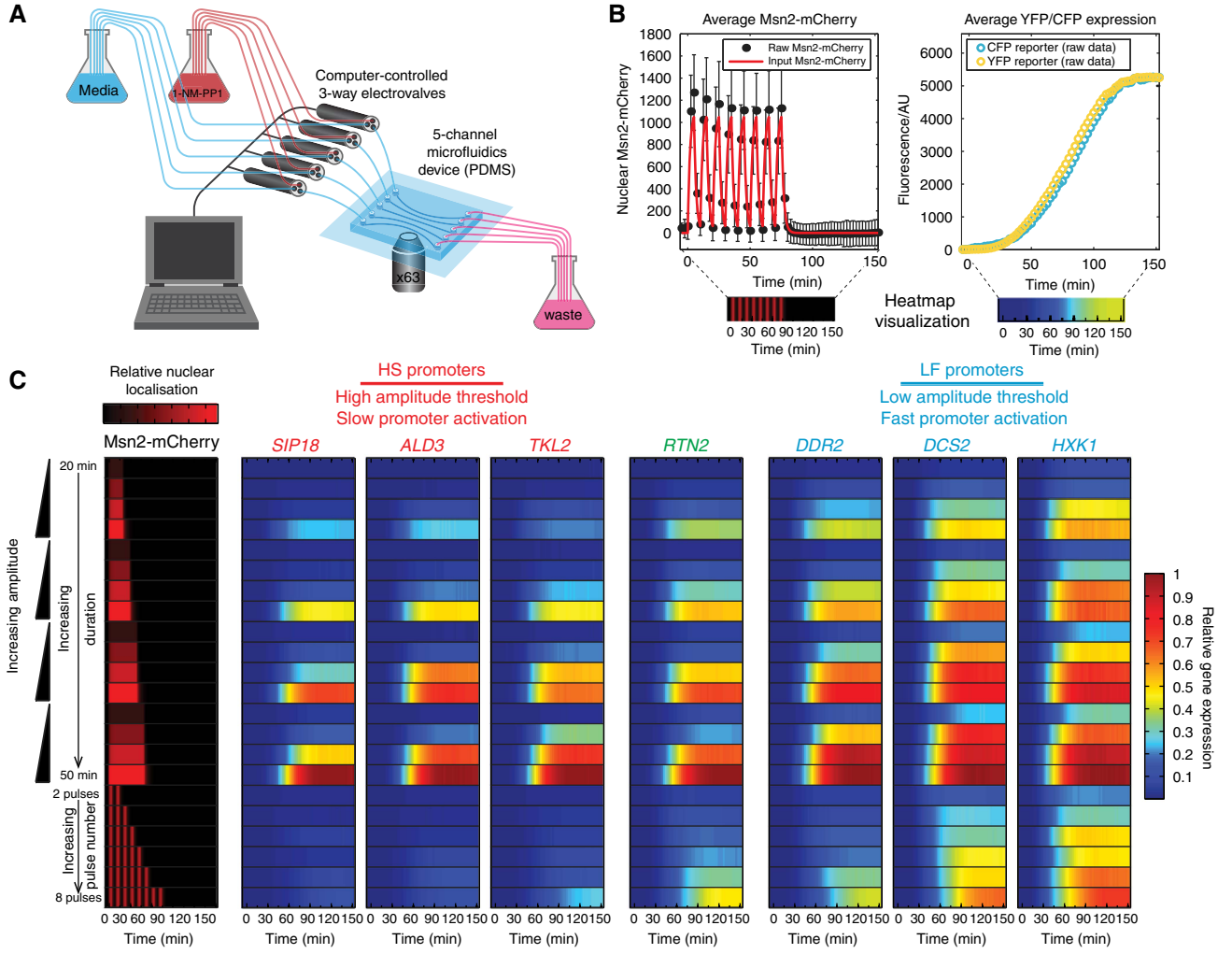

Figure 1 Experimental set-up and systematic dissection of how different promoters decode TF dynamics. (**A**) Microfluidic set-up. Medium with or without the PKA^{as} inhibitor 1-NM-PP1 is delivered to five computer-controlled 3-way electrovalves. These control when and for how long each microfluidic channel receives 1-NM-PP1. Simultaneously, a 63x microscope objective moves between each microfluidic channel and records Msn2-mCherry translocation dynamics and gene expression in single cells. (**B**) An example of an experiment (*DDR2*). Cells were treated with eight 5 min pulses of 1-NM-PP1 with 5 min intervals (red line: input Msn2-mCherry) and Msn2-mCherry translocation dynamics were monitored in single diploid cells (black dots: raw data). Gene expression was monitored with fast maturing dual CFP (SCFP3A) and YFP (mCitrineV163A) reporters. (**C**) Systematic dissection of how different promoters decode TF dynamics. Each row corresponds to a specific Msn2-mCherry input (left, in red) and the corresponding gene expression response for each of the seven promoters is shown on the corresponding rows on the right. The gene expression responses for each promoter are internally normalized to their maximal expression level. Each row is the per-cell average of ~200–600 cells from at least three biological replicates. The promoter classification is derived from their clustering (Figure 2B). The full data sets are given in Supplementary Figure S1D. Source data for this figure are available on the online Supplementary information page.

single cells with high temporal resolution (example experiment: Figure 1B and Supplementary Movie 1).

For each of the 7 promoters, we performed 30 experiments in which we systematically modulated the amplitude, duration, pulse number, and pulse interval of Msn2 nuclear localization (Supplementary Figure S1D) to mimic the naturally observed Msn2 translocation dynamics in response to stress (Hao and O'Shea, 2012). We observed significant differences between the promoters (Figure 1C): *SIP18, TKL2,* and *ALD3* filtered out low amplitude input (25 and 50% amplitude), short duration input and oscillatory input, and only induced in response to sustained high-amplitude input; in contrast, *HXK1, DCS2,* and *DDR2* responded strongly to short oscillatory input and short duration input, while showing saturation at high amplitude. In between these extremes, *RTN2* filtered out low amplitude input like *SIP18*, yet showed significant induction in response to short duration and oscillatory input like *DDR2* (Figure 1C). Thus, natural promoters decode the same TF input differently.

Using a mathematical model to cluster promoters into classes

To provide a quantitative framework for understanding the input–output relationship between Msn2 dynamics and gene expression, we constructed a mathematical model for TF-activated gene expression using ordinary differential

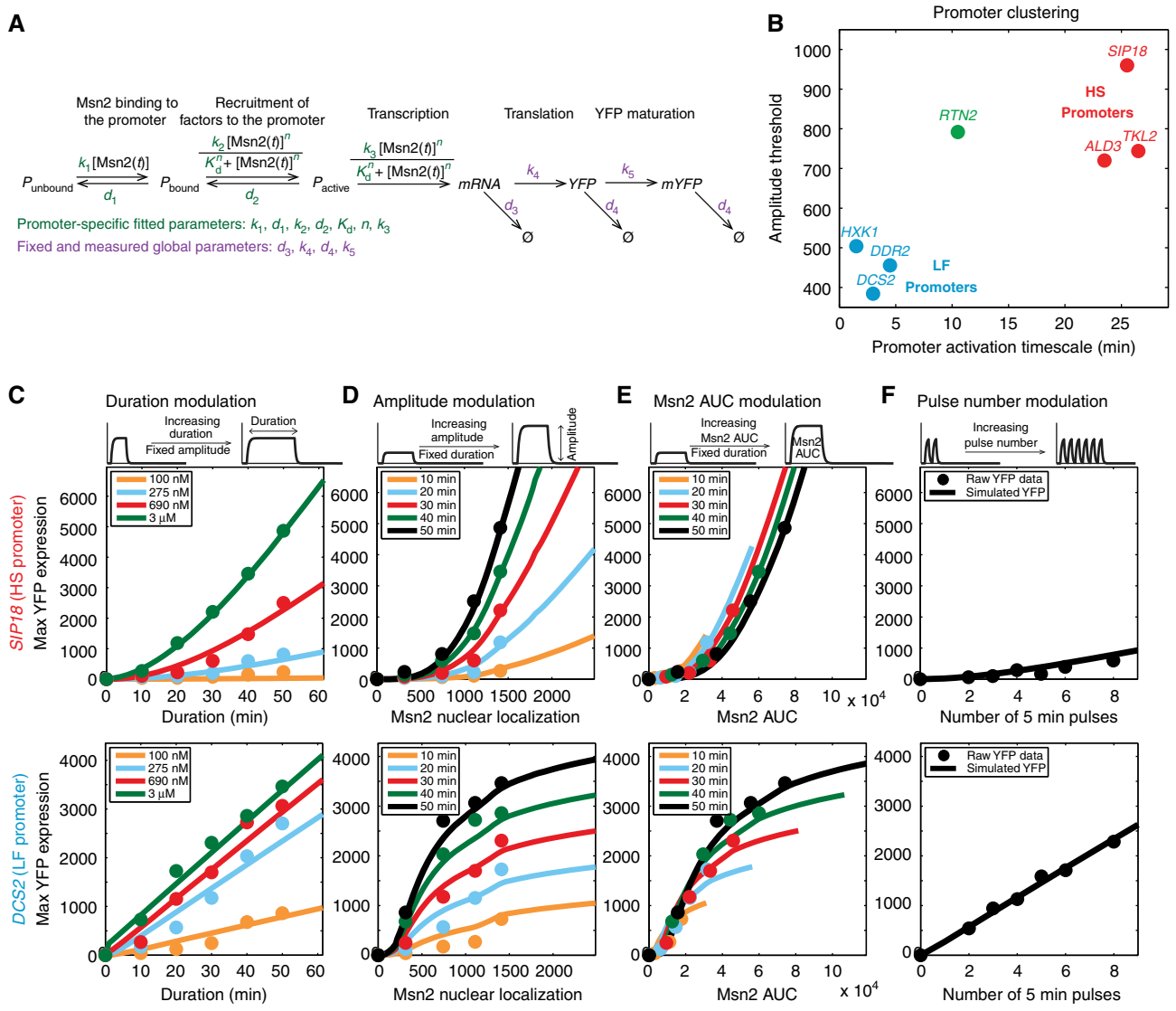

Figure 2 A mathematical model for transcription factor-activated gene expression allows clustering of promoters and detailed quantitative characterization. (**A**) A mathematical model (defined by the differential equations in Materials and methods). Promoter-specific parameters shown in green were obtained by least-squares global fitting to the full data set (Supplementary Figure S1D) using the Msn2-mCherry traces as input and the YFP traces as output. Parameters shown in purple are the same for all promoters and were experimentally determined. (**B**) Clustering of promoters. The amplitude threshold is defined as the nuclear Msn2-mCherry level required to reach half the P_{active} level obtained at 3 μM 1-NM-PP1 (which corresponds to the maximal nuclear Msn2-mCherry level) and obtained by mathematical simulations using the model in (**A**). The promoter activation timescale is defined as the time (min) it takes to reach half the steady-state P_{active} level at 690 nM 1-NM-PP1 and was also obtained from model simulations. (**C**–**F**) Illustration of how *SIP18* and *DCS2* respond to duration, amplitude, Msn2 AUC, and pulse number modulation. In all cases, the dots represent raw data (the maximum of the average YFP time trace under the specific conditions) and the curves (lines) were obtained from mathematical simulations using the best-fit parameters and the model in (**A**). In (**C**), 100 nM, 275 nM, 690 nM, and 3 μM are 1-NM-PP1 concentrations corresponding to *ca.* 25, 50, 75, and 100% Msn2-mCherry nuclear localization. In (**D**, **E**), the duration was fixed to 10, 20, 30, 40, or 50 min and the amplitude increased until 2500 AU. In (**E**), Msn2 AUC is defined as the time-integrated nuclear localization, that is, the area under the curve. In (**F**), both the pulse duration and the pulse interval are 5 min. See Supplementary Figures S2–S5 for full comparisons of model fitting to raw data and Supplementary Table S2 for parameters. Source data for this figure are available on the online Supplementary information page.

equations (Figure 2A). Rather than pursuing an all-encompassing mechanistic model that would differ between promoters, we selected from several candidates the simplest model that could accurately describe all of the promoters despite their very different behavior (see Supplementary information). Models with only two promoter states could not adequately account for the long activation delay that we observe for *SIP18, ALD3,* and *TKL2*. Thus, our final model contains three promoter states. Although these are phenomenological variables rather than biochemically well-defined promoter states, we interpret these as unbound, bound, and active: initially, the promoter is unbound and the rate with which Msn2 binds the promoter is assumed to be proportional to the nuclear concentration of Msn2. Once bound, recruitment of factors to the promoter ($P_{bound} \rightarrow P_{active}$) is assumed to be proportional to the equilibrium fraction of Msn2 bound to the promoter and modeled as a Hill function. To account for the observation that transcription ceases when

Msn2 exits the nucleus, we also model transcription as a Hill function (a full discussion of the model is given in Supplementary information).

To extract quantitative information, we identified the parameter set (green parameters in Figure 2A) that gave the best overall fit to the full 30-experiment data set (Supplementary Figures S2–S5) for each promoter. Global parameters (purple parameters in Figure 2A) were experimentally determined and found not to differ between promoters (see Supplementary information). Using the model and the fitted parameters, we calculated the promoter activation timescale (time required to reach the half-maximal P_{active} level) and amplitude threshold (amplitude required to reach the half-maximal P_{active} level at steady state) for each promoter. We clustered the promoters along these two axes and observed classes of behavior (Figure 2B). *HXK1*, *DCS2,* and *DDR2* belong to one promoter class, which we call Low amplitude threshold, Fast promoters (LF promoters, blue)—these promoters activate within a few minutes, which explains why they respond strongly to short duration oscillatory input (Figure 1C). Due to their low amplitude threshold, LF promoters show strong gene expression responses even to low amplitude input and show saturation at high amplitude input. At the other extreme, *SIP18*, *ALD3*, and *TKL2* belong to a class we call High amplitude threshold, Slow promoters (HS promoters, red)—due to their long activation delay (~25 min), they filter out short duration input, including short duration oscillatory input (Figure 1C). Similarly, due to their high amplitude threshold, low amplitude input is filtered out regardless of the duration.

Finally, *RTN2* shows intermediate behavior: *RTN2* filters out low amplitude input like the HS promoters (Figure 1C) and has a promoter activation timescale (~10 min) in between that of the LF and HS promoters, but more similar to the LF promoters. The response of *RTN2* to short oscillatory input is similar to *DDR2* (Figure 1C). Hence, *RTN2* exhibits much faster activation than *TKL2* and *ALD3*, but a higher amplitude threshold: this shows that amplitude threshold and promoter activation timescale can be at least partially decoupled. We therefore predict that natural promoters will show a continuum in response behavior and span the entire space of Figure 2B, including all four corners.

Quantitative analysis of signal processing by LF and HS promoters

To illustrate how the HS and LF promoter classes process TF signals, we quantitatively analyzed *SIP18* (HS) and *DCS2* (LF). In response to duration modulation (Figure 2C, dots: raw data; lines: model simulations), *SIP18* expression increases in a nonlinear, convex manner due to its slow promoter activation and shows a duration threshold below which no gene expression is seen. *DCS2* expression, on the other hand, increases linearly with duration due to its fast activation and shows no threshold. The highly convex scaling of *SIP18* in response to amplitude modulation (Figure 2D) shows how sensitive its expression is to the amplitude: an ~25% increase in amplitude can more than double gene expression output. In contrast, *DCS2* shows concave scaling and begins to show saturation even at the half-maximal amplitude. When expression is plotted as a function of the Msn2 AUC (Msn2 area under the curve, $\int_0^\infty [\text{Msn2}(t)]\text{d}t$), we see a clear threshold (*ca*. 2×10^4 Msn2 AUC, Figure 2E) below which *SIP18* filters out all input, whereas *DCS2* shows no such threshold. Instead, *DCS2* expression is simply proportional to the Msn2 AUC until saturation—after saturation *DCS2* expression is no longer sensitive to increasing amplitude. Thus, even for single pulse input, natural Msn2 target promoters can act as sophisticated signal processing modules with distinct decoding abilities.

Finally, in response to pulse number modulation, *DCS2* expression is simply proportional to the number of pulses (Figure 2F)—this is because promoter activation and deactivation are so fast that no memory effects are observed between the pulses (Hao and O'Shea, 2012). *SIP18,* on the other hand, displays such slow promoter activation kinetics that oscillatory input is largely filtered out regardless of the pulse number.

Control of TF dynamics enables differential gene expression

Having established that different promoter classes decode TF dynamics differently, we next investigated whether this would allow differential gene expression. Using the model (Figure 2A), we systematically simulated gene expression for different input dynamics (duration, amplitude, pulse number, and pulse interval) for *SIP18* and *DCS2*. The model predicts that strong induction of *DCS2* without significant induction of *SIP18* can be achieved by using short, low frequency oscillatory input (Figure 3A, Condition A). Likewise, the model predicts that differential expression of *SIP18* over *DCS2* can be achieved by using a single sustained, high amplitude pulse (Figure 3B, Condition B).

We tested these model predictions by measuring gene expression in response to these two conditions and find that the model could accurately predict gene expression responses to conditions upon which it had not been trained (Figure 3). This demonstrates that significant differential gene expression between LF and HS promoters at an absolute level is possible just by controlling TF dynamics. Thus, the cell can exploit this mechanism to encode multiple, distinct gene expression programs in the translocation dynamics of a single TF.

Noise in gene expression differs markedly for different promoter classes and depends on Msn2 dynamics

Having analyzed how gene expression responses depend on Msn2 input at the population level, we next investigated single-cell behavior. Since the dual CFP and YFP reporters share the same cellular environment, the degree to which they correlate allows us to discern two sources of cell-to-cell variability (Elowitz *et al*, 2002): variability caused by the shared environment, such as differences in the number of Msn2 molecules or ribosomes between cells, which affect both CFP and YFP equally (extrinsic noise); and the remaining intrinsic variability that is not accounted for by the shared environment, which may stem from factors such as stochastic

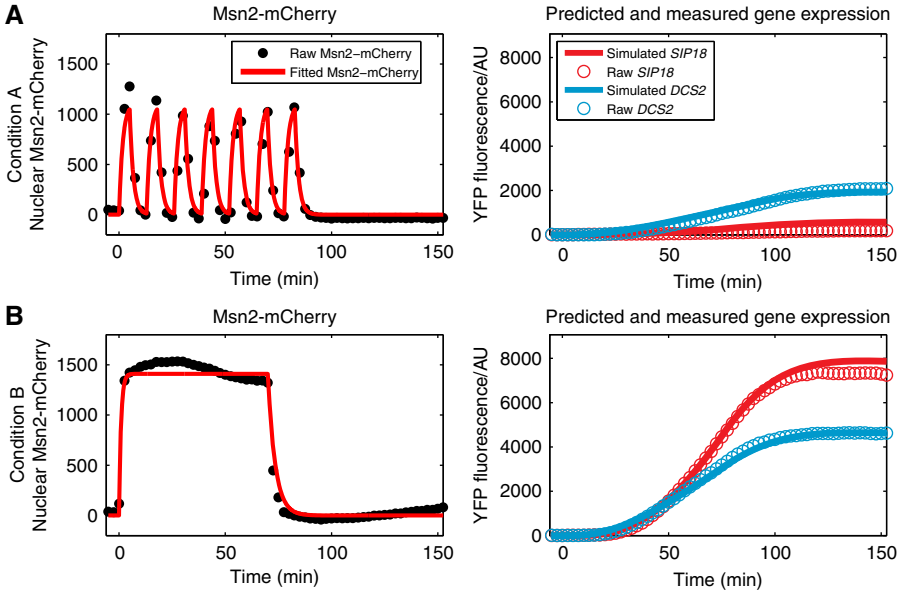

Figure 3 Control of TF dynamics allows differential gene expression. (**A**, **B**) The left column shows the Msn2-mCherry input and the right column shows the predicted gene expression responses to that Msn2-mCherry input (simulated using the model in Figure 2A) and the raw experimentally measured gene expression data for the *SIP18* and *DCS2* reporters (per-cell average of ~300–500 cells). Condition A: seven 5 min pulses separated by 7.95 min at 690 nM 1-NM-PP1. Condition B: a single 70-min pulse at 3 μM 1-NM-PP1. See Supplementary Figure S6 for raw single-cell data. Source data for this figure are available on the online Supplementary information page.

binding events at individual promoters (intrinsic noise) (Hilfinger and Paulsson, 2011).

We first investigated how total (Figure 4A) and intrinsic (Figure 4B) noise (σ^2/μ^2) scale with TF input (Msn2 AUC) for all experiments for all seven promoters (each dot in Figure 4A and B corresponds to the gene expression noise for a given Msn2 input for a single promoter (colored by class)). Although noise generally decreases with increasing Msn2 AUC, we observed substantial differences in total and intrinsic noise between the promoter classes: for a given Msn2 AUC, noise in gene expression was significantly higher for the slow (HS) promoters than the fast (LF) promoters. Since the Msn2 input, mRNA transcript (coding region and 3′ UTR) and protein are the same for all promoters, differences in intrinsic noise between promoters should primarily originate from promoter transitions and transcription. Therefore, different promoter classes exhibit inherently different levels of noise in gene expression. For example, even when *SIP18* (HS) expression robustly exceeds *DCS2* (LF) expression at the population level (Figure 3B), *SIP18* still exhibits more than two-fold higher noise than *DCS2* (Supplementary Figure S6B).

To determine whether noise in gene expression depends on TF dynamics, we compared the total noise for a single 40-min pulse with eight 5 min oscillatory pulses (Figure 4C) such that the Msn2 AUC, total duration, and amplitude were constant. We find that noise in gene expression is higher in response to oscillatory input than in response to a single pulse. Furthermore, the extent to which oscillatory input results in higher noise seems to depend on the promoter class: HS promoters are much noisier in general, but also show greater differences between oscillatory input and single pulse input. This contrasts with a recent theoretical study (Tostevin *et al*, 2012), which found that at steady state, oscillatory input could lead to lower noise than constant input. However, this discrepancy is likely due to differences in comparisons: that study used a much higher amplitude for oscillatory input than for constant input such that the promoter activation timescale was shorter for oscillatory input (see also Supplementary information).

Notably, the only promoter that shows a negligible noise difference between oscillatory and single pulse input is *HXK1*, which also has the fastest activation timescale (~1.3 min). In fact, the noise (Figure 4C, orange bars) is significantly correlated with the promoter activation timescale ($\rho = 0.919$; $P < 0.005$; Pearson's correlation), such that the slower the promoter activation, the higher the noise.

Single-cell time traces (Figure 4D and E) and a CFP/YFP scatterplot (Figure 4F) for *DCS2* and *SIP18* illustrate how substantial the noise differences are between the HS and LF promoters. We find that both intrinsic and extrinsic noise contribute significantly to the total noise. For *DCS2*, gene expression is remarkably reliable with low variation between cells. For *SIP18*, however, we observe bimodal gene expression: some cells induce very strongly, whereas a large proportion of cells show no expression at all. In general, we observe many cases of bimodal gene expression for the HS promoters when the signal is close to the threshold (Supplementary Figure S7H and J), which further underscores how noisy these promoters are.

Taken together, our results reveal that oscillatory TF input leads to higher noise in gene expression and that noise is significantly correlated with the promoter activation timescale. That HS promoters suffer from significantly higher total and intrinsic noise than LF promoters furthermore implies an inherent trade-off: employing HS and LF promoters enables differential gene expression by controlling TF dynamics; but for the HS promoter, high noise means that the information encoded in TF dynamics is decoded with low fidelity.

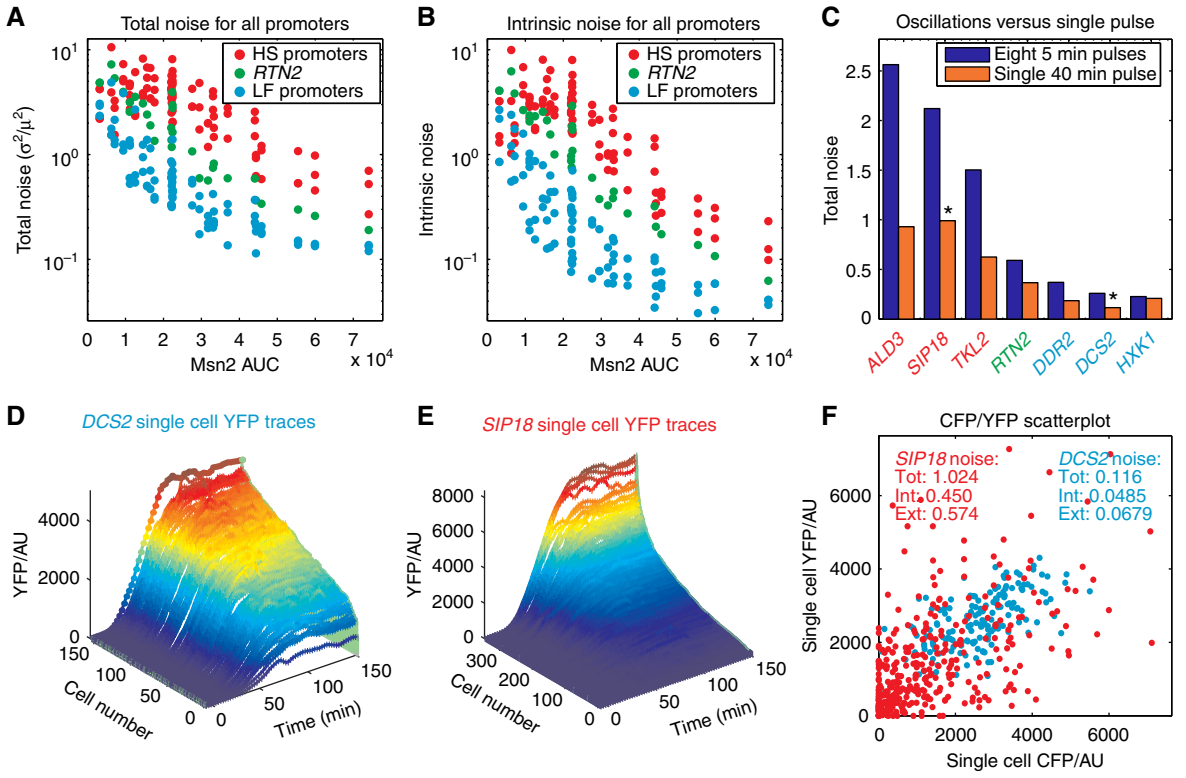

Figure 4 Noise in gene expression depends on the promoter class and on TF dynamics. (**A**, **B**) Total noise (**A**) (σ^2/μ^2) and intrinsic (**B**) noise (defined in Materials and methods) is plotted against the Msn2 AUC (red, green, and blue denotes HS (*SIP18*, *ALD3* and *TKL2*), *RTN2*, and LF (*DDR2*, *DCS2*, and *HXK1*) promoters, respectively). Each dot corresponds to the noise (mean noise across time points after gene expression has reached a plateau) for a single experiment: that is, a single Msn2 input for a single promoter. (**C**) TF dynamics and noise. The total noise for a 40-min pulse at 690 nM 1-NM-PP1 (purple) is compared with the total noise for eight pulses with 5 min duration and interval at 690 nM 1-NM-PP1 (orange) such that the total Msn2 AUC is constant. (**D**, **E**) Single-cell YFP time traces for *DCS2* and *SIP18* in response to a single 40-min pulse at 690 nM 1-NM-PP1 corresponding to the orange bar graphs for *DCS2* and *SIP18* in (**C**) that are highlighted with an asterisk (*). The traces show raw single-cell YFP data (smoothed by a 3-point moving average). (**F**) YFP/CFP scatterplot. Each dot corresponds to the raw CFP (*x* axis) and YFP (*y* axis) fluorescence in a single cell at 150 min from (**D**) and (**E**). *SIP18:* red dots. *DCS2*: blue dots. Spread along the diagonal is due to extrinsic noise effects and spread orthogonal to the diagonal is due to intrinsic noise effects. See also Supplementary Figure S7 for examples of bimodal gene expression, noise versus mean, extrinsic noise and additional plots. Source data for this figure are available on the online Supplementary information page.

Encoding four gene expression programs in the dynamics of a single TF

Previously, we showed that natural promoters differ in their amplitude threshold and promoter activation timescale and, importantly, that these two properties can be decoupled (Figure 2B). On the basis of these observations, four promoter classes exist in theory: promoters can have either a low or a high amplitude threshold (H or L) and exhibit either fast or slow activation (F or S). To theoretically investigate whether differential expression of all four classes is possible by controlling TF dynamics, we consider the simplest formulation of the deterministic model (Figure 5A) that can capture differences in both the amplitude threshold and promoter activation timescales of the full model (Figure 2A). We quantify gene expression as the mRNA AUC (Figure 5B), which will be proportional to the protein level after it has reached a plateau since the mRNA lifetime is much shorter than the protein lifetime.

Next, we generate representative promoters for each of the four classes *in silico* that differ only in their amplitude threshold and promoter activation timescale (Figure 5C). We analytically solve the model for the mRNA AUC (see Supplementary information) and then systematically investigate how gene expression depends on duration, amplitude, pulse interval, and pulse duration (Supplementary Figure S8A–C). By searching this space, we identify four conditions where differential expression of the four promoters at an absolute level is possible. The HS promoter dominates in response to a single sustained, high-amplitude pulse (Figure 5D, left), the LS promoter dominates in response to a single sustained, low-amplitude pulse (Figure 5E), the LF promoter dominates in response to low amplitude, low frequency oscillations (Figure 5F), and finally, the HF promoter dominates in response to high amplitude, low frequency oscillations (Figure 5G). Thus, it is possible to encode four distinct gene expression programs in the translocation dynamics of a single TF.

The promoter activation timescale controls the noise level

Experimentally, we observed a strong positive correlation between noise and the promoter activation timescale. Consistent with this result, in the case of the four *in silico*

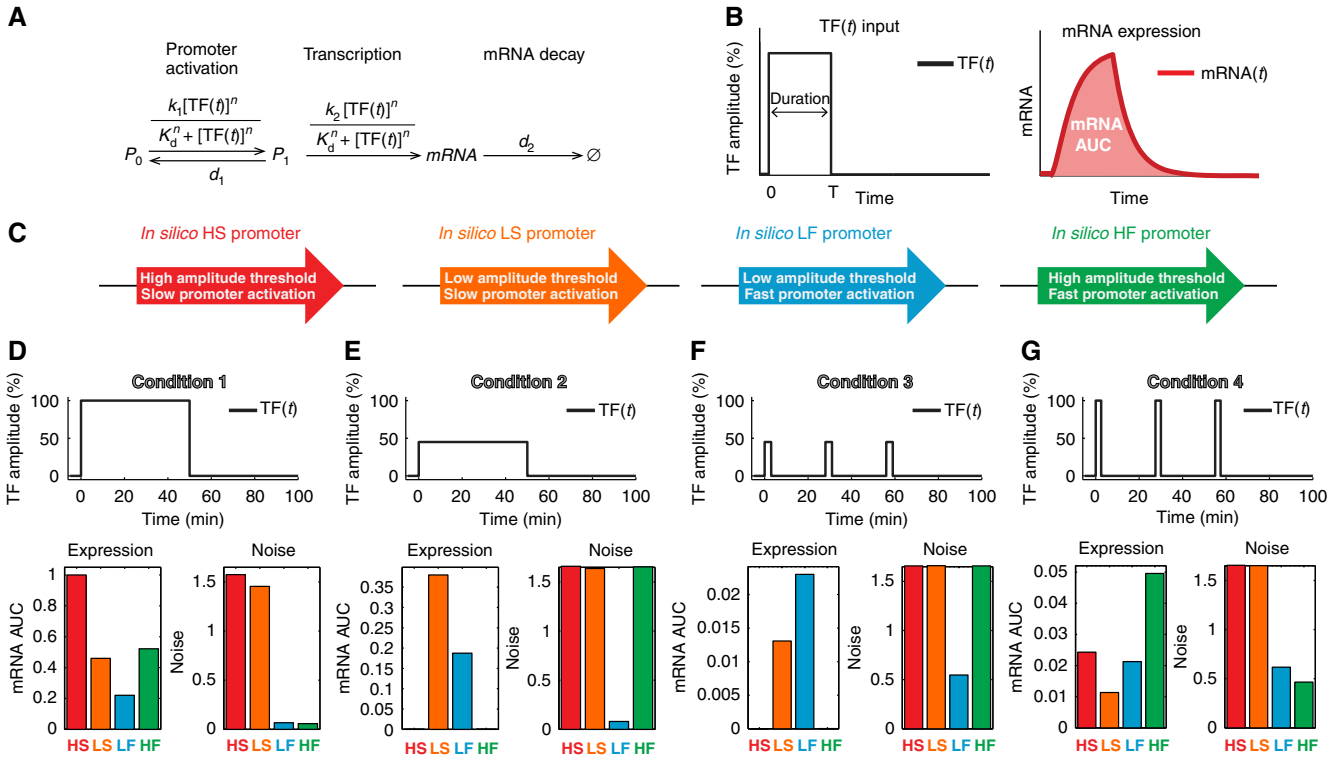

Figure 5 Encoding four gene expression programs in the dynamics of a single TF. (**A**) A simplified model. (**B**) TF input (left) and gene expression output (mRNA AUC, right) for the model in (**A**). Nuclear translocation is modeled as a step function and gene expression is quantified as the mRNA AUC. (**C**) Analysis of *in silico* promoters. Four hypothetical promoters were generated *in silico* and their sensitivity to TF dynamics analyzed. Parameters were chosen such that the timescale of the promoter transition for the slow and fast promoters were on as same order as *SIP18* (~30 min) and *HXK1* (~1 min), respectively. The following parameters were used: $k_1 = d_1 = 0.0167$ (HS, LS), $k_1 = d_1 = 0.5$ (HF, LF), $K_d = 75$, $n = 8$ (HS, HF), $K_d = 20$, $n = 2.5$ (HS, HF), $k_2 = 30$ (HS), $k_2 = 12$ (LS), $k_2 = 3$ (LF), $k_2 = 8$ (HF), $d_2 = 0.12\ \text{min}^{-1}$(for all). (**D**–**G**) Differential gene expression and noise. Four conditions were chosen such that each of the four promoters would show higher gene expression (mRNA AUC, left bar graph) than the other three under one condition. The gene expression values were globally normalized to one, such that the differences shown are absolute and not just relative. The mRNA AUC noise (σ^2/μ^2, right bar graph in **D**–**G**) was obtained from exact discrete-time stochastic simulations (10^5 iterations) of the model in (**A**) for each condition and promoter. The noise *y* axis maximum was set to 1.65 in all cases because under multiple conditions (e.g., Condition 2 and 3 for HS), the gene expression is essentially zero and the noise essentially infinite. Full surface plots showing how gene expression and noise scale with TF amplitude, nuclear duration, pulse duration and interval can be found in Supplementary Figure S8. A discussion of the model and its solution is given in Supplementary information.

promoters (Figure 5D–G, right and Supplementary Figure S8D–F), the LF promoter always exhibits lower noise than the LS promoter and the HF promoter always exhibits lower noise than the HS promoter. Furthermore, the noise levels we observe for the slow promoters (Figure 4) are substantially higher than those typically seen in steady-state studies (Bar-Even *et al*, 2006; Newman *et al*, 2006). To understand why, consider a fast (HF or LF) and a slow (LS or HS) promoter exposed to a single, transient pulse: for all but the briefest pulses, all fast promoters in a population will activate and approach a new steady state, whereas for a slow promoter a substantial fraction will not even activate in response to a sustained pulse (50 min, Figure 6A). During a 50-min pulse, the fast promoter will frequently switch between the ON and the OFF states, such that although there is variability in the amount of time it is active during the pulse, the variability between cells is relatively modest (Figure 6B): all promoters are active for at least 10 min, but none for >40 min. For the slow promoter, however, 43% of cells fail to activate at all (Figure 6B); and among the fraction that do activate, because of the slow switching frequency, the variability in the amount of time the promoter is active is huge (Figure 6B). This explains why slow promoter kinetics leads to such high noise.

This is also consistent with many previous steady-state studies that have shown that genes with high transcriptional burst frequency but small burst sizes exhibit lower noise than genes with low burst frequency but large burst sizes (Raj and van Oudenaarden, 2008; Hornung *et al*, 2012; Lionnet and Singer, 2012; Dadiani *et al*, 2013). Comparing promoters with the same mean expression, but different kinetics, we find that noise scales strongly with the activation timescale (Figure 6C). But as the pulse duration approaches that of two cell divisions (~200 min, steady-state behavior), the effect of the promoter activation timescale on noise is greatly reduced. Therefore, whereas at steady state the effects of promoter kinetics (burst frequency) are modest because of averaging due to the long lifetimes of proteins, the consequences are dramatic when the pulse is transient (Figure 6C). Thus, the promoter activation timescale controls noise in gene expression and this underscores the importance of promoter kinetics when considering transient TF dynamics.

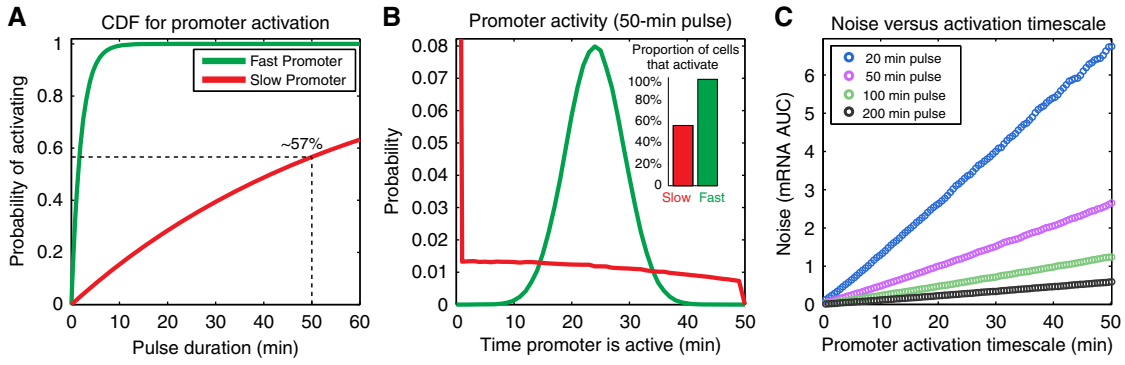

Figure 6 Gene expression noise depends on the promoter activation timescale. (**A**) Cumulative distribution function (CDF) versus pulse length. The CDF describes the proportion of cells that activate at least once during a pulse. Parameters: fast promoter ($k_1 = d_1 = 0.5$); slow promoter ($k_1 = d_1 = 0.0167$). (**B**) Promoter activity histogram. For a 50-min pulse, the histogram shows the variability in the amount of time the fast (green) and slow (red) promoters are active. For the slow promoter, ~43% of cells fail to activate at all. Simulated using the Gillespie algorithm (10^6 iterations). (**C**) Noise versus activation timescale. Using the model in (Figure 5A) and $k_1 = d_1 = (0.0098;1.00)$, $K_d = 20$, $n = 2.5$, $k_2 =$ from 3 and upwards, $d_2 = 0.12$ per min. Each data point is from discrete-time stochastic simulations (5×10^4 iterations). k_2 was chosen such that, for a given pulse duration, the mean expression is constant for all activation timescales.

Slower promoter activation leads to greater noise in gene expression

A key prediction of our theory is that slowing down promoter activation will lead to higher noise. Since TFs generally cannot bind to binding sites in the promoter that are occupied by nucleosomes (Lam *et al*, 2008; Zhou and O'Shea, 2011) and nucleosome removal often accompanies gene induction (Shivaswamy *et al*, 2008; Bai *et al*, 2010), we hypothesized that interfering with chromatin remodeling would slow down promoter activation. To test this, we generated strains lacking either the SWI/SNF (*snf6*Δ) or the SAGA (*gcn5*Δ) chromatin remodeling complexes (Raser and O'Shea, 2004) and containing the *SIP18* and *HXK1* expression reporters.

For the *SIP18* reporter, both complexes are required for induction (Supplementary Figure S9C). For the SWI/SNF and SAGA mutants of the *HXK1* reporter strain, the expression level is not substantially affected so we repeated all 30 experiments (Supplementary Figure S9A) and fit the model (Figure 2A) to the data to obtain parameters from which we inferred the amplitude threshold and promoter activation timescale (Figure 7A). Both mutants showed slower promoter activation (Figure 7A) and higher noise (Figure 7B–D) consistent with our previous observations (Figure 4) and theoretical predictions (Figures 5 and 6). Furthermore, as observed for the natural promoters (Figure 4C), the slower *HXK1* mutants now show higher noise in response to oscillatory than single pulse input, whereas the faster WT strain does not (Figure 7D). Overall, we conclude that the promoter activation timescale is a key determinant of noise in gene expression.

Nucleosome remodeling dynamics correlate with promoter activation dynamics

The observation that chromatin remodeling complex mutants slow down promoter activation led us to hypothesize that nucleosome remodeling might be rate limiting for promoter activation. To test this, we used micrococcal nuclease digestion coupled with high-throughput sequencing (MNase-Seq) to follow nucleosome remodeling dynamics in response to Msn2 activation (Figure 7E). We find that whereas all promoters have clearly positioned nucleosomes initially, nucleosome positioning collapses within 5 min for the fast *HXK1* and *DCS2* promoters (a hallmark of transcriptional activation; Zhou and O'Shea, 2011). In contrast, slow promoters such as *SIP18* have higher nucleosome occupancy initially and the nucleosomes remain clearly positioned until the 20–30 min time points which is very similar to the activation timescale we inferred using modeling (~25 min, Figure 2B). The observed correlation between nucleosome remodeling and promoter activation is consistent with a model where the promoter activation timescale is controlled by the position and stability of promoter nucleosomes.

Discussion

Promoter amplitude threshold and activation timescale control how TF dynamics are decoded

The expanding list of TFs that exhibit complicated dose- and signal-dependent dynamics prompted us to systematically investigate the quantitative principles that govern how gene promoters decode such dynamics. We demonstrate that the amplitude threshold and promoter activation timescale govern how TF dynamics are decoded. But at the mechanistic level, what determines these two properties? From previous steady-state studies, it appears that the amplitude threshold depends at least in part on the binding affinity of the promoter for the TF; that is, the affinity and number of TF binding sites and chromatin structure (Lam *et al*, 2008; Sharon *et al*, 2012). This is also consistent with our observations: LF promoters tend to have multiple clustered Msn2 binding sites, whereas *RTN2* and HS promoters tend to have only one or two isolated sites (Supplementary Figure S9D). Much less is known about what determines the promoter activation timescale. We show here that the model-inferred promoter activation timescales largely match the observed nucleosome remodeling timescales. Furthermore, we show that the SWI/SNF and SAGA chromatin

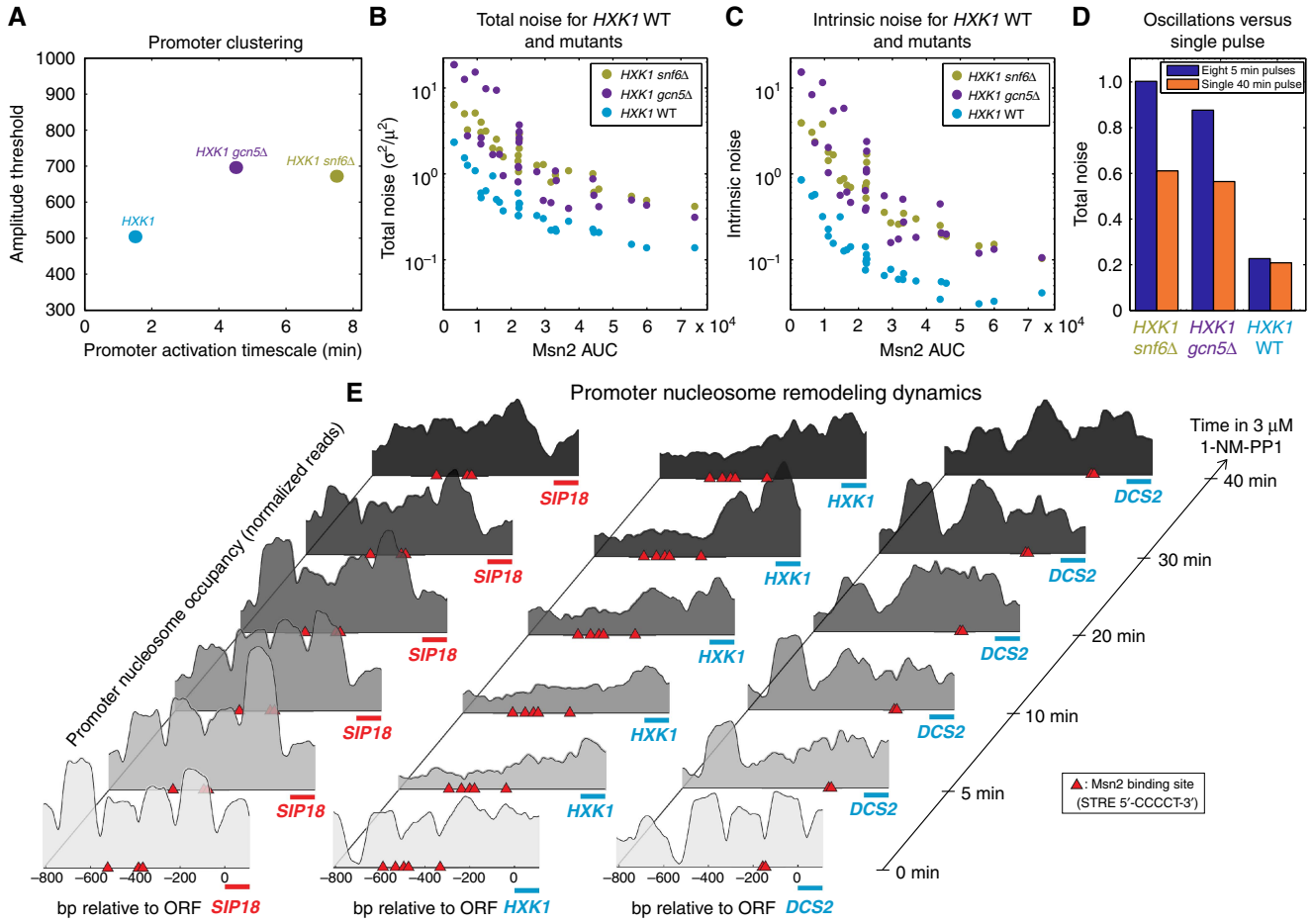

Figure 7 Slower promoter activation kinetics leads to greater noise in gene expression. (**A**) Promoter clustering of chromatin remodeling complex mutants (*SWI/SNF* (*snf6*Δ) and *SAGA* (*gcn5*Δ)). All 30 experiments (Supplementary Figure S9A) were repeated in biological triplicate for the mutant strains and their amplitude threshold and promoter activation timescale obtained from fitting to the deterministic model in (Figure 2A). (**B**, **C**) Total (**B**) and intrinsic noise (**C**) for *HXK1* WT, *HXK1 snf6*Δ and *HXK1 gcn5*Δ strains as a function of Msn2 AUC. (**D**) The total noise for a 40-min pulse at 690 nM 1-NM-PP1 (purple) is compared with the total noise for eight pulses with 5 min duration and interval at 690 nM 1-NM-PP1 (orange) such that the total Msn2 AUC is constant. (**E**) Nucleosome remodeling dynamics. Promoter nucleosome occupancy in response to 3 μM 1-NM-PP1 was profiled using MNase-Seq (see Supplementary information). See also Supplementary Figure S9 for the full data sets and additional nucleosome data. Source data for this figure are available on the online supplementary information page.

remodeling complexes are required for the induction of *SIP18* and that deleting them significantly slows down activation of the *HXK1* promoter (Figure 7). Taken together, a coarse grained model emerges where the amplitude threshold is related to TF binding sites and the promoter activation timescale to nucleosome organization. Detailed mechanistic studies are now required to elucidate the details of what determines the amplitude threshold and promoter activation timescale at individual promoters. Such studies, however, should be greatly facilitated by the high-throughput technologies developed here.

Modulation of TF dynamics enables control of gene expression

Using mathematical modeling, we predict and experimentally verify conditions where differential expression of two promoters is possible at an absolute level (Figure 3), providing evidence that TF dynamics is an important mechanism for control of gene expression. We extend this result to four promoter classes by showing theoretically (Figure 5D–G) how absolute differential expression of the HS, LS, LF, and HF promoter classes can be achieved by controlling only TF dynamics. Mammalian TFs appear to be constrained in the number of distinct binding sites that can be evolved (Berger *et al*, 2008). Thus, in addition to combinatorial regulation, an economical way of overcoming this limitation might be for the cell to encode multiple gene expression programs in the dynamics of a single TF rather than evolving multiple TFs with distinct binding site specificities.

Relationship between promoter class and stress-specific gene function

Msn2 dynamics qualitatively differ in response to glucose starvation, osmotic and oxidative stress (Hao and O'Shea,

2012). Although the genes in this study were chosen because their transcriptional response is strong and Msn2 specific, is there a relationship between gene function and promoter class? For two of the genes we studied, based on the gene function, we can rationalize why a given gene might belong to a given class. For example, the HS promoter *SIP18* will filter out the brief pulses of nuclear Msn2 during glucose starvation, and will induce only during prolonged nuclear accumulation of Msn2 that occurs in oxidative stress, where the protein appears to protect against reactive oxygen species (Rodriguez-Porrata *et al*, 2012). Conversely, the fast LF promoter *HXK1* responds strongly to brief pulses and will induce strongly during glucose starvation, where the protein catalyzes phosphorylation of glucose and facilitates growth on non-fermentable carbon sources (Herrero *et al*, 1995). For several of the other genes, the function or stress requirement is unclear. Thus, while the correlation between gene function and promoter class is intuitive for *SIP18* and *HXK1*, a larger sample size will be necessary to determine whether this correlation is general rather than anecdotal.

Using our synthetic PKA^{as} system, we studied the causal input–output relationship between artificially controlled Msn2 dynamics and the promoter-controlled gene expression response. However, in response to natural stresses, factors other than Msn2 will be activated and the regulation may be partly post-transcriptional. Thus, while we show that exploiting the four promoter classes is sufficient to encode four gene expression programs in the dynamics of a single TF, complementary approaches will be required to determine how much of the physiological regulation for natural stresses is promoter class controlled and how much is post-transcriptional or Msn2 independent.

A trade-off between noise and control of gene expression

Previous studies on TF dynamics did not consider gene expression noise (Cai *et al*, 2008; Hao and O'Shea, 2012). Here, we provide a link between TF dynamics and control of noise in gene expression: for constant amplitude, total duration, and TF AUC, oscillatory input gives rise to higher noise in gene expression than a single pulse. This shows that noise depends on TF dynamics and that the function of TF oscillations is unlikely to be the reduction of noise in gene expression (Tostevin *et al*, 2012). Instead, given that low frequency oscillations enables the cell to induce LF and HF promoters without inducing LS and HS promoters, it is likely that this advantage of low frequency oscillations overrides the cost of higher noise in gene expression.

Furthermore, noise also depends on the promoter class—the slower the promoter activation timescale, the greater the noise in gene expression. These promoter class-specific noise and decoding properties highlight a key trade-off for the cell (Figure 8). Any signal transduction pathway has to distinguish real signals from noise and transmit the intensity of the signal. This invariably carries the risk of false signals being transmitted. HS promoters have filtering abilities when decoding signals and reliably filter out such noise up to a threshold. In contrast, LF promoters are activated immediately and transmit such signaling noise (Figure 8A). Conversely, HS promoters respond strongly to a real signal, but with high gene expression noise. LF promoters, on the other hand, are inherently less noisy and respond reliably with low noise (Figure 8B). Thus, there is a clear trade-off between promoters having filtering abilities and low noise in gene expression.

This further reveals that the cell faces an important trade-off between encoding multiple gene expression programs in TF dynamics and having them decoded with high fidelity (low noise): with four promoter classes, cells can encode up to four distinct gene expression programs in the dynamics of a single TF. Yet, the two slow promoter classes (LS and HS) inherently suffer from high noise in gene expression, which severely limits their decoding fidelity.

Previous work on p53 and NF-κB have divided their target genes into 'early' versus 'late' categories depending on their qPCR-measured induction dynamics (Tay *et al*, 2010; Purvis *et al*, 2012). In the case of p53, the late genes are associated with terminal cell fates such as senescence and apoptosis (Purvis *et al*, 2012). The results presented here would place these 'late' genes in the HS or LS classes and predict that they would filter out the sporadic pulses that have been shown to occur in cycling cells (Loewer *et al*, 2010) and thereby avoid the aberrant induction of apoptosis, but also that they would suffer from high noise in gene expression when actually induced. Since the failure to induce these terminal cell fate genes could result in the development of cancer and the death of the organism, this further underscores how serious this trade-off between noise and control of gene expression can be (Figure 8).

One of the central challenges that the cell faces is how to transmit information in such a way that the desired responses are elicited. Systems engineering faces much the same challenge. We show here that individual promoters can serve as discrete signal-processing modules that the cell can exploit to decode TF dynamics: by tuning their amplitude threshold promoters can filter out low amplitude input (*SIP18*), simply integrate the signal (*DCS2* before saturation) or filter out high amplitude input (*DCS2* after saturation); by tuning their promoter activation timescale promoters can serve as high-pass filters (low frequency TF input is filtered out), signal integrators (fast promoters), or duration filters (slow promoters). Furthermore, we connect each signal-processing module (promoter class) with signal decoding fidelity: the ability to filter out short duration and low frequency TF input comes at the cost of high noise in gene expression. Hence, although the cell can choose between several distinct signal-processing modules when decoding TF dynamics, there is a trade-off between noise and control of gene expression.

Materials and methods

Strains

The yeast strains used in this study are in the W303 background and a full list can be found in Supplementary Table S1. Full details on strain construction are given in Supplementary information.

Microarray analysis and reporter gene selection

To determine the transcriptional target genes of Msn2, genome-wide gene expression levels in response to 3 μM of 1-NM-PP1 were analyzed

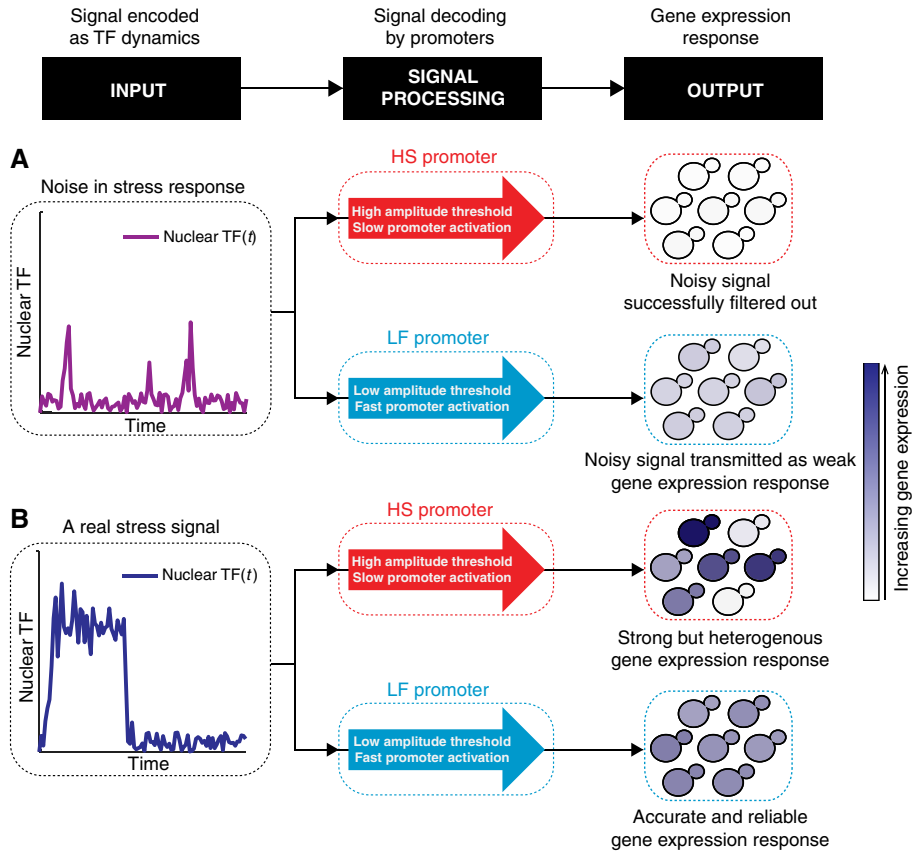

Figure 8 A trade-off between noise and control of gene expression. (**A**) Natural variation along the baseline in a stress response signal transduction pathway can lead to spurious activation of a transcription factor (signaling noise). The high-threshold HS promoter filters out such noise, whereas the fast LF promoter transmits such upstream noise as a weak gene expression response. (**B**) A real stress signal is transmitted for decoding by both promoters. The LF promoter is inherently less noisy and yields a strong and accurate gene expression response. The HS promoter is inherently noisy and yields a strong, but heterogenous gene expression response.

in a diploid Msn2-mCherry strain and compared with a diploid *msn2*Δ strain. Cells were grown overnight to an $OD_{600\,nm}$ of 0.15 and 1-NM-PP1 was added to a final concentration of 3 μM. Cells were harvested at time points 0, 10, 20, and 40 min and RNA extraction, cDNA synthesis, microarray hybridization (Agilent 8 × 15 K *S. cerevisiae* two-color arrays), and data normalization performed as previously described (Zhou and O'Shea, 2011). Genes that showed at least five-fold upregulation in response to 1-NM-PP1 in the Msn2-mCherry diploid, but no expression change in the *msn2*Δ diploid (Supplementary Figure S1C) and no serious deletion phenotype were selected and their endogenous ORF replaced by SCFP3A or mCitrineV163A followed by the ADH1 terminator and dual-reporter diploids formed by mating. Of these diploid strains, seven showed strong enough expression for reliable detection by microscopy. All seven promoters are known to directly bind Msn2 (Huebert *et al*, 2012). Full details are given in Supplementary information.

Microfluidic device

The high-throughput device developed here was loosely inspired by a previously reported low-throughput device (Hersen *et al*, 2008). Briefly, the SU8 master wafer was fabricated using standard photolithography technology and custom transparency masks and the PDMS-based microfluidic device produced by replica molding using standard soft lithography techniques. Each microfluidic channel has a width of 400 μm and a height of *ca*. 111 μm. The design for the transparency mask is available upon request. Full details are given in Supplementary information.

Time-lapse microscopy

Yeast cells were grown overnight at 30°C to an $OD_{600\,nm}$ of 0.1, quickly collected by filtration and loaded into a microfluidic device pre-treated with concanavalin A. Five 3-way electrovalves (LFYA1228032H Y-valve in perfluoroelastomer, the Lee Company) control whether normal medium or medium with 1-NM-PP1 is delivered to each of the five microfluidic channels and the flow (*ca*. 1 μl/s per channel) driven by gravity. The valves can be computationally switched within milliseconds and the medium inside the microfluidic channel changed within seconds. The device was loaded on a Zeiss AxioObserver Z1 inverted microscope with an EM-CCD camera and the entire system was kept at 30°C. Images were acquired with an oil-immersion objective (63x, NA 1.4, oil Ph3, Plan-Apochromat) with 2.5 min resolution for 64 frames. The automated microscope stage moves between the positions, maintains focus, and acquires phase contrast, YFP, CFP, iRFP, and RFP images. To monitor Msn2-mCherry nuclear localization, a z-stack series (focal plane ± 1.75 μm) was acquired. The electrovalves were programmed with custom-written software (MATLAB) that is available upon request. Full details are given in Supplementary information.

Image analysis

Image analysis was performed using custom-written software (MATLAB) that automatically segments, tracks, and quantifies single cells. Briefly, the cell segmentation algorithm fits the best ellipse from a library to the cell boundary. The background subtraction algorithm uses the mode in each channel. The tracking algorithm proceeds by

matching closest cells between frames subject to a series of constraints. The nucleus is segmented by thresholding the NHP6a-iRFP nuclear marker. Quantification of nuclear Msn2-mCherry is done by considering the brightest pixels in a maximum-intensity projection of an Msn2-mCherry z-stack series. CFP (SCFP3A) and YFP (mCitrineV163A) reporter expression was adjusted for photobleaching and quantified as the mean pixel intensity of the entire cell. The image analysis code is available upon request. Full details are given in Supplementary information.

Deterministic model

The model (Figure 2A) consists of the three promoter states, mRNA, pre-mature YFP and mature YFP, and is described by the following six ordinary differential equations:

$$\frac{dP_{unbound}}{dt} = d_1 P_{bound} - k_1[\mathrm{Msn2}(t)]P_{unbound} \quad (1)$$

$$\frac{dP_{bound}}{dt} = k_1[\mathrm{Msn2}(t)]P_{unbound} + d_2 P_{active} - \left(d_1 + \frac{k_2[\mathrm{Msn2}(t)]^n}{K_d^n + [\mathrm{Msn2}(t)]^n}\right)P_{bound} \quad (2)$$

$$\frac{dP_{active}}{dt} = \frac{k_2[\mathrm{Msn2}(t)]^n}{K_d^n + [\mathrm{Msn2}(t)]^n} P_{bound} - d_2 P_{active} \quad (3)$$

$$\frac{d[\mathrm{mRNA}]}{dt} = \frac{k_3[\mathrm{Msn2}(t)]^n}{K_d^n + [\mathrm{Msn2}(t)]^n} P_{active} - d_3[\mathrm{mRNA}] \quad (4)$$

$$\frac{d[\mathrm{YFP}]}{dt} = k_4[\mathrm{mRNA}] - (d_4 + k_5)[\mathrm{YFP}] \quad (5)$$

$$\frac{d[m\mathrm{YFP}]}{dt} = k_5[\mathrm{YFP}] - d_4[m\mathrm{YFP}] \quad (6)$$

The input function is $[\mathrm{Msn2}(t)]$, which is a continuous function that describes how Msn2 nuclear localization changes with time and the output is *m*YFP. A full discussion of the model and how the fitting was performed is given in Supplementary information. The parameters for each promoter are listed in Supplementary Table S2.

Gene expression noise definitions

Following the dual-reporter convention for two reporters x and y (Elowitz *et al*, 2002), the total, extrinsic, and intrinsic noise are defined as:

$$\eta^2_{total} = \frac{\langle x^2 + y^2\rangle - 2\langle x\rangle\langle y\rangle}{2\langle x\rangle\langle y\rangle}$$

$$\eta^2_{ext} = \frac{\langle xy\rangle - \langle x\rangle\langle y\rangle}{\langle x\rangle\langle y\rangle}$$

$$\eta^2_{int} = \frac{\langle (x-y)^2\rangle}{2\langle x\rangle\langle y\rangle}$$

where the angled brackets denote averaging over the entire cell population. In all cases where noise is reported in this study, the noise is the mean of multiple time points after the gene expression trace has reached its plateau. For the dual-reporter system to work, the CFP and YFP reporters must be statistically identically distributed. Due to inherent differences in brightness and exposure times, it is necessary to rescale the CFP values by multiplication of a constant factor. This resulted in the CFP and YFP reporters having the same mean and distributions.

In vivo nucleosome mapping (MNase-Seq)

Cells were grown overnight to an $OD_{600\,nm}$ of 0.15 and 1-NM-PP1 was added to a final concentration of 3 μM. Cells were harvested at time points 0, 5, 10, 20, 30, and 40 min. Crosslinking, lysis, MNase digestion, mononucleosome purification, and sequencing library preparation were performed as previously described (Zhou and O'Shea, 2011). Paired-end libraries were sequenced on an Illumina Hiseq 2000 and bioinformatic analysis performed using Perl, Python, and MATLAB. Full details are given in Supplementary information.

Synthesis of 1-NM-PP1

1-NM-PP1 was synthesized from 1-naphthaleneacetic acid in five chemical steps at a gram-scale (>99% pure by NMR) using standard methods from organic synthesis. Full synthetic details are given in Supplementary information.

Accession codes

Illumina sequencing data are available in the ArrayExpress database (www.ebi.ac.uk/arrayexpress) under accession number E-MTAB-1950. Microarray data are available in the ArrayExpress database under accession number E-MTAB-1945.

Supplementary information

Supplementary information is available at the *Molecular Systems Biology* website (www.nature.com/msb).

Acknowledgements

We thank N Hao for insightful discussions. We thank X Zhou, S Mukherji, RV Wadhwani, D MacLaurin and members of the O'Shea laboratory for discussions. We thank J Paulsson, B Stern, D Huh, V Denic and members of the O'Shea laboratory for critically reading the manuscript. This work was performed in part at the Center for Nanoscale Systems at Harvard University, a member of the National Nanotechnology Infrastructure Network (NNIN), which is supported by the National Science Foundation under NSF award no. ECS-0335765. The Howard Hughes Medical Institute supported this work.

Author contributions: ASH and EKO designed the project. ASH conducted the experiments and analyzed the data. ASH and EKO wrote the manuscript.

Conflict of interest

The authors declare that they have no conflict of interest.

References

Ashall L, Horton CA, Nelson DE, Paszek P, Harper CV, Sillitoe K, Ryan S, Spiller DG, Unitt JF, Broomhead DS, Kell DB, Rand DA, See V, White MR (2009) Pulsatile stimulation determines timing and specificity of NF-kappaB-dependent transcription. *Science* **324:** 242–246

Bai L, Charvin G, Siggia ED, Cross FR (2010) Nucleosome-depleted regions in cell-cycle-regulated promoters ensure reliable gene expression in every cell cycle. *Dev Cell* **18:** 544–555

Balaban NQ, Merrin J, Chait R, Kowalik L, Leibler S (2004) Bacterial persistence as a phenotypic switch. *Science* **305:** 1622–1625

Bar-Even A, Paulsson J, Maheshri N, Carmi M, O'Shea E, Pilpel Y, Barkai N (2006) Noise in protein expression scales with natural protein abundance. *Nat Genet* **38:** 636–643

Batchelor E, Loewer A, Mock C, Lahav G (2011) Stimulus-dependent dynamics of p53 in single cells. *Mol Syst Biol* **7:** 488

Behar M, Hoffmann A (2010) Understanding the temporal codes of intra-cellular signals. *Curr Opin Genet Dev* **20:** 684–693

Berger MF, Badis G, Gehrke AR, Talukder S, Philippakis AA, Pena-Castillo L, Alleyne TM, Mnaimneh S, Botvinnik OB, Chan ET, Khalid F, Zhang W, Newburger D, Jaeger SA, Morris QD, Bulyk ML, Hughes TR (2008) Variation in homeodomain DNA binding revealed by high-resolution analysis of sequence preferences. *Cell* **133:** 1266–1276

Bishop AC, Ubersax JA, Petsch DT, Matheos DP, Gray NS, Blethrow J, Shimizu E, Tsien JZ, Schultz PG, Rose MD, Wood JL, Morgan DO, Shokat KM (2000) A chemical switch for inhibitor-sensitive alleles of any protein kinase. *Nature* **407:** 395–401

Brennan MD, Cheong R, Levchenko A (2012) How information theory handles cell signaling and uncertainty. *Science* **338:** 334–335

Cai L, Dalal CK, Elowitz MB (2008) Frequency-modulated nuclear localization bursts coordinate gene regulation. *Nature* **455:** 485–490

Covert MW, Leung TH, Gaston JE, Baltimore D (2005) Achieving stability of lipopolysaccharide-induced NF-kappa B activation. *Science* **309:** 1854–1857

Dadiani M, van Dijk D, Segal B, Field Y, Ben-Artzi G, Raveh-Sadka T, Levo M, Kaplow I, Weinberger A, Segal E (2013) Two DNA-encoded strategies for increasing expression with opposing effects on promoter dynamics and transcriptional noise. *Genome Res* **23:** 966–976

Elowitz MB, Levine AJ, Siggia ED, Swain PS (2002) Stochastic gene expression in a single cell. *Science* **297:** 1183–1186

Giorgetti L, Siggers T, Tiana G, Caprara G, Notarbartolo S, Corona T, Pasparakis M, Milani P, Bulyk ML, Natoli G (2010) Noncooperative Interactions between Transcription Factors and Clustered DNA Binding Sites Enable Graded Transcriptional Responses to Environmental Inputs. *Mol Cell* **37:** 418–428

Gorner W, Durchschlag E, Martinez-Pastor MT, Estruch F, Ammerer G, Hamilton B, Ruis H, Schuller C (1998) Nuclear localization of the C2H2 zinc finger protein Msn2p is regulated by stress and protein kinase A activity. *Gene Dev* **12:** 586–597

Hao N, O'Shea EK (2012) Signal-dependent dynamics of transcription factor translocation controls gene expression. *Nat Struct Mol Biol* **19:** 31–U47

Herrero P, Galindez J, Ruiz N, Martinezcampa C, Moreno F (1995) Transcriptional regulation of the Saccharomyces cerevisiae Hxk1, Hxk2 and Glk1 genes. *Yeast* **11:** 137–144

Hersen P, McClean MN, Mahadevan L, Ramanathan S (2008) Signal processing by the HOG MAP kinase pathway. *Proc Natl Acad Sci USA* **105:** 7165–7170

Hilfinger A, Paulsson J (2011) Separating intrinsic from extrinsic fluctuations in dynamic biological systems. *Proc Natl Acad Sci USA* **108:** 12167–12172

Hornung G, Bar-Ziv R, Rosin D, Tokuriki N, Tawfik DS, Oren M, Barkai N (2012) Noise-mean relationship in mutated promoters. *Genome Res* **22:** 2409–2417

Huebert DJ, Kuan PF, Keles S, Gasch AP (2012) Dynamic changes in nucleosome occupancy are not predictive of gene expression dynamics but are linked to transcription and chromatin regulators. *Mol Cell Biol* **32:** 1645–1653

Jacquet M, Renault G, Lallet S, De Mey J, Goldbeter A (2003) Oscillatory nucleocytoplasmic shuttling of the general stress response transcriptional activators Msn2 and Msn4 in Saccharomyces cerevisiae. *J Cell Biol* **161:** 497–505

Lahav G, Rosenfeld N, Sigal A, Geva-Zatorsky N, Levine AJ, Elowitz MB, Alon U (2004) Dynamics of the p53-Mdm2 feedback loop in individual cells. *Nat Genet* **36:** 147–150

Lam FH, Steger DJ, O'Shea EK (2008) Chromatin decouples promoter threshold from dynamic range. *Nature* **453:** 246–U216

Lionnet T, Singer RH (2012) Transcription goes digital. *EMBO Rep* **13:** 313–321

Loewer A, Batchelor E, Gaglia G, Lahav G (2010) Basal dynamics of p53 reveal transcriptionally attenuated pulses in cycling cells. *Cell* **142:** 89–100

Nelson DE, Ihekwaba AE, Elliott M, Johnson JR, Gibney CA Foreman BE, Nelson G, See V, Horton CA, Spiller DG, Edwards SW, McDowell HP, Unitt JF, Sullivan E, Grimley R, Benson N, Broomhead D, Kell DB, White MR (2004) Oscillations in NF-kappaB signaling control the dynamics of gene expression. *Science* **306:** 704–708

Newman JRS, Ghaemmaghami S, Ihmels J, Breslow DK, Noble M, DeRisi JL, Weissman JS (2006) Single-cell proteomic analysis of S. cerevisiae reveals the architecture of biological noise. *Nature* **441:** 840–846

Petrenko N, Chereji RV, McClean M, Morozov AV, Broach JR (2013) Noise and interlocking signaling pathways promote distinct transcription factor dynamics in response to different stresses. *Mol Biol Cell* **24:** 2045–2057

Purvis JE, Karhohs KW, Mock C, Batchelor E, Loewer A, Lahav G (2012) p53 dynamics control cell fate. *Science* **336:** 1440–1444

Purvis JE, Lahav G (2013) Encoding and decoding cellular information through signaling dynamics. *Cell* **152:** 945–956

Raj A, Peskin CS, Tranchina D, Vargas DY, Tyagi S (2006) Stochastic mRNA synthesis in mammalian cells. *PLoS Biol* **4:** 1707–1719

Raj A, van Oudenaarden A (2008) Nature, nurture, or chance: stochastic gene expression and its consequences. *Cell* **135:** 216–226

Raser JM, O'Shea EK (2004) Control of stochasticity in eukaryotic gene expression. *Science* **304:** 1811–1814

Rodriguez-Porrata B, Carmona-Gutierrez D, Reisenbichler A, Bauer M, Lopez G, Escote X, Mas A, Madeo F, Cordero-Otero R (2012) Sip18 hydrophilin prevents yeast cell death during desiccation stress. *J Appl Microbiol* **112:** 512–525

Sharon E, Kalma Y, Sharp A, Raveh-Sadka T, Levo M, Zeevi D, Keren L, Yakhini Z, Weinberger A, Segal E (2012) Inferring gene regulatory logic from high-throughput measurements of thousands of systematically designed promoters. *Nat Biotechnol* **30:** 521–530

Shivaswamy S, Bhinge A, Zhao YJ, Jones S, Hirst M, Iyer VR (2008) Dynamic remodeling of individual nucleosomes across a eukaryotic genome in response to transcriptional perturbation. *PLoS Biol* **6:** 618–630

Tay S, Hughey JJ, Lee TK, Lipniacki T, Quake SR, Covert MW (2010) Single-cell NF-kappaB dynamics reveal digital activation and analogue information processing. *Nature* **466:** 267–271

Tostevin F, de Ronde W, Ten Wolde PR (2012) Reliability of frequency and amplitude decoding in gene regulation. *Phys Rev Lett* **108:** 108104

Werner SL, Barken D, Hoffmann A (2005) Stimulus specificity of gene expression programs determined by temporal control of IKK activity. *Science* **309:** 1857–1861

Yissachar N, Fischler TS, Cohen AA, Reich-Zeliger S, Russ D Shifrut E, Porat Z, Friedman N (2013) Dynamic response diversity of NFAT isoforms in individual living cells. *Mol Cell* **49:** 322–330

Zaman S, Lippman SI, Schneper L, Slonim N, Broach JR (2009) Glucose regulates transcription in yeast through a network of signaling pathways. *Mol Syst Biol* **5:** 245

Zhou X, O'Shea EK (2011) Integrated approaches reveal determinants of genome-wide binding and function of the transcription factor Pho4. *Mol Cell* **42:** 826–836